Inorganic Chemistry

Article

Single-Molecule Magnetism Properties of the First Strontium-Manganese Cluster [SrMn₁₄O₁₁(OMe)₃(O₂CPh)₁₈(MeCN)₂]

Abhudaya Mishra,[†] **Yulia Pushkar,**[‡] **Junko Yano,**[‡] **Vittal K. Yachandra,**[‡] **Wolfgang Wernsdorfer,**[§] **Khalil A. Abboud,**[†] **and George Christou*,**[†]

Department of Chemistry, University of Florida, Gainesville, Florida 32611, Melvin Calvin Laboratory, Physical Biosciences Division, Lawrence Berkeley National Laboratory, Berkeley, California 94720, and Institut Néel, CNRS/UJF, BP 166, 25 Avenue des Martyrs, 38042 Grenoble Cedex 9, France

The preparation and properties of the first strontium-manganese molecular complex are described. The reaction of $(NBu^n_4)[Mn_4O_2(O_2CPh)_9(H_2O)]$ (4Mn^{III}) with $Sr(ClO_4)_2$ in MeCN/MeOH led to the isolation of $[SrMn_{14}O_{11}(OMe)_3(O_2CPh)_{18}(MeCN)_2]$ (**1**; 13Mn^{III}, Mn^{II}). The structure of **1** consists of two $[Mn_4O_3(OMe)]$ cubane units attached to a central, near-planar, trinuclear $[Mn_3O_4]$ unit, to which are also attached a Mn and a Sr above the plane and a $[Mn_2O(OMe)]$ rhomb below the plane. Peripheral ligation is provided by 18 bridging benzoate and two terminal MeCN groups. Variable-temperature and -field dc magnetization (M) data were collected in the 1.8–10 K and 0.1–4.0 T ranges and fit by matrix diagonalization methods to give $S = 9/2$, $D = -0.50(5)$ cm⁻¹, and $g = 1.88(10)$, where S is the ground-state spin and D is the axial zero-field splitting parameter. Magnetization versus dc field sweeps at various temperatures and scan rates exhibited hysteresis loops, confirming **1** to be a new single-molecule magnet. Because complex **1** is the initial molecular example of intimately associated Mn and Sr atoms, Sr EXAFS studies have been performed for the first time on a synthetic Sr-containing molecule. This has also allowed comparisons with the EXAFS data on the Sr-substituted water oxidizing complex (WOC) of Photosystem II (PS II), which contains a SrMn₄ complex.

Introduction

Molecular manganese carboxylate cluster chemistry continues to attract a lot of attention from many groups around the world. The reasons for this are many, but the two most important ones are the relevance of the chemistry of this metal to Mn bioinorganic chemistry and to the ongoing efforts to develop new routes to nanoscale magnetic materials. The latter area primarily involves the synthesis of single-molecule magnets (SMMs), which are molecules that retain their magnetization below a blocking temperature (T_B) in the absence of an applied field.[1,2] This thus represents a molecular, "bottom-up" approach to nanoscale magnets, complementary to the standard "top-down" approaches to nanoparticles of traditional magnetic materials such as certain metals and metal oxides. For a molecule to function as an SMM, it must possess a large ground-state spin (S) and a negative (easy-axis or Ising) magnetoanisotropy (D). Together, these provide a barrier to relaxation of the magnetization vector whose upper limit is given by $S^2|D|$ and $(S^2 - ¼)|D|$ for integer and half-integer spins, respectively. Several classes of SMMs are now known,[3] most of them being Mn^{III}-containing species, since the Jahn–Teller distortion of this oxidation state represents a major source of the molecular anisotropy. Nevertheless, there is a continuing need to identify new SMMs, either by developing methods to modify

 * To whom correspondence should be addressed. Tel: (352) 392-8314.Fax: (352) 392-8757. E-mail: christou@chem.ufl.edu.
 † University of Florida.
 ‡ Lawrence Berkeley National Laboratory.
 § Institut Néel.

 (1) (a) Christou, G.; Gatteschi, D.; Hendrickson, D. N.; Sessoli, R. *MRS Bull.* **2000**, *25*, 66 and references cited therein. (b) Christou, G. *Polyhedron* **2005**, *24*, 2065.

 (2) (a) Sessoli, R.; Tsai, H. L.; Schake, A. R.; Wang, S.; Vincent, J. B.; Folting, K.; Gatteschi, D.; Christou, G.; Hendrickson, D. N. *J. Am. Chem. Soc.* **1993**, *115*, 1804. (b) Sessoli, R.; Gatteschi, D.; Caneschi, A.; Novak, M. A. *Nature* **1993**, *365*, 141. (c) Soler, M.; Chandra, S. K.; Ruiz, D.; Davidson, E. R.; Hendrickson, D. N.; Christou, G. *Chem. Commun.* **2000**, 2417. (d) Boskovic, C.; Pink, M.; Huffman, J. C.; Hendrickson, D. N.; Christou, G. *J. Am. Chem. Soc.* **2001**, *123*, 9914. (e) Aubin, S. M. J.; Sun, Z.; Guzei, I. A.; Rheingold, A. L.; Christou, G.; Hendrickson, D. N. *J. Chem. Soc., Chem. Commun.* **1997**, 2239.

known structural types or by synthesizing completely new ones, or both. Such an expansion of the number of known SMMs types is important in order to improve our understanding of this interesting phenomenon.

In the bioinorganic field, the water oxidizing complex (WOC) in Photosystem II (PS II) catalyzes water oxidation to O_2 gas in green plants and cyanobacteria.[4,5] The WOC is an oxide-bridged $CaMn_4$ cluster containing primarily Mn^{III} and Mn^{IV} ions and mainly carboxylate peripheral ligation. It requires Ca^{2+} for activity,[6] and Ca EXAFS (extended X-ray absorption fine structure) studies have revealed a Mn···Ca separation of ∼3.4 Å.[7] Also studied by many groups is the Sr^{2+}-substituted WOC,[8,9] Sr being the only metal that can substitute for the Ca^{2+} with major retention of activity (∼40%);[8] a corresponding Mn···Sr separation of ∼3.5 Å has been detected by Sr EXAFS studies.[9] Recent crystallographic studies on the PS II reaction center of the cyanobacterium *Thermosynechococcus elongatus* at 3.5 Å[10] and 3.0 Å[11] resolution, and more recent polarized EXAFS studies have confirmed the WOC to be a mixed-metal Mn_4Ca complex.[12] Although there is some uncertainty about the extent of any radiation damage during X-ray data collection,[11,13] there is little doubt overall that the WOC is heterometallic.[10,11]

In the present work, we have sought new Mn clusters that might be SMMs by incorporating the large group 2 metal, strontium. This follows on from our recent work in mixed-metal Ca/Mn studies reported elsewhere,[14a] which provided the first example of an intimately associated molecular Ca/Mn cluster of higher oxidation state Mn; there are still very few Ca/Mn species.[14] Similarly, there are no molecular Sr/Mn clusters currently known, only some polymeric Sr^{II}/Mn^{II} species.[15] Therefore, we have been investigating mixed Sr/Mn chemistry as a potential route to new magnetically interesting clusters and have successfully prepared a molecular $SrMn_{14}$ complex. This paper reports the structural and magnetic characterization of this compound, which identifies the compound as a new single-molecule magnet, and the results of its characterization by Sr EXAFS studies, which have also allowed some comparisons with data on the Sr-substituted WOC. Portions of this work have been previously communicated.[16]

Experimental Section

Syntheses. All manipulations were performed under aerobic conditions using chemicals as received, unless otherwise stated. $(NBu^n_4)[Mn_4O_2(O_2CPh)_9(H_2O)]$ was prepared as described elsewhere.[17]

$[SrMn_{14}O_{11}(OMe)_3(O_2CPh)_{18}(MeCN)_2]$ (1). To a stirred solution of $(NBu^n_4)[Mn_4O_2(O_2CPh)_9(H_2O)]$ (0.50 g, 0.31 mmol) in MeCN/MeOH (20/2 mL) was slowly added $Sr(ClO_4)_2 \cdot xH_2O$ (0.089 g, 0.31 mmol). The dark brown solution was stirred for a further 20 min, filtered, and the filtrate slowly concentrated by evaporation at ambient temperature, which slowly produced dark red crystals of **1·12 MeCN** over two days. The yield was 55%. The crystals of **1** were maintained in the mother liquor for X-ray crystallography and other single-crystal studies, or collected by filtration, washed with MeCN, and dried in vacuo. The synthesis can also be carried out with $Sr(NO_3)_2$. The vacuum-dried solid was analyzed as solvent-free. Elemental analysis: Calcd (Found) for **1** ($C_{133} H_{105}Mn_{14}Sr_1 N_2O_{50}$): C, 47.15 (46.92); H, 3.12 (2.92); N, 0.83 (0.63). Selected IR data (KBr, cm^{-1}): 3430(br), 2968(w), 1600(m), 1559(m), 1405(s), 1177(w), 1069(w), 1025(w), 841(w), 715(s), 676(m), 615(m), 503(w).

X-ray Crystallography. Data were collected on a Siemens SMART PLATFORM equipped with a CCD area detector and a

(3) (a) Selected examples of SMMs: Mn,[3b] Fe,[3c] Ni,[3d] Co,[3e] mixed-metal,[3f–k] and lanthanide.[3l] (b) Tasiopoulos, A. J.; Vinslava, A.; Wernsdorfer, W.; Abboud, K. A.; Christou, G. *Angew. Chem., Int. Ed.* **2004**, *43*, 2117. (c) Jones, L. F.; Low, D. M.; Helliwell, M.; Raftery, J.; Collison, D.; Aromi, G.; Cano, J.; Mallah, T.; Wernsdorfer, W.; Brechin, E. K.; McInnes, E. J. L. *Polyhedron* **2006**, *25*, 325. (d) Bell, A.; Aromi, G.; Teat, S. J.; Wernsdorfer, W.; Winpenny, R. E. P. *Chem. Commun.* **2005**, 2808. (e) Yang, E. C.; Hendrickson, D. N.; Wernsdorfer, W.; Nakano, M.; Zakharov, L. N.; Sommer, R. D.; Rheingold, A. L.; Ledezma-Gairaud, M.; Christou, G. *J. Appl. Phys.* **1991**, *91*, 7382. (f) Mishra, A.; Wernsdorfer, W.; Abboud, K. A.; Christou, G. *J. Am. Chem. Soc.* **2004**, *126*, 15648. (g) Zaleski, C. M.; Depperman, E. C.; Kampf, J. W.; Kirk, M. L.; Pecoraro, V. L. *Angew. Chem., Int. Ed.* **2004**, *43*, 3912. (h) Schelter, E. J.; Prosvirin, A. V.; Dunbar, K. R. *J. Am. Chem. Soc.* **2004**, *126*, 15004. (i) Oshio, H.; Nihei, M.; Koizumi, S.; Shiga, T.; Nojiri, H.; Nakano, M.; Shirakawa, N.; Akatsu, M. *J. Am. Chem. Soc.* **2005**, *127*, 4568. (j) Sokol, J. J.; Hee, A. G.; Long, J. R. *J. Am. Chem. Soc.* **2002**, *124*, 7656. (k) Murugesu, M.; Mishra, A.; Wernsdorfer, W.; Abboud, K. A.; Christou, G. *Polyhedron* **2006**, *25*, 613. (l) Ishikawa, N.; Sugita, M.; Wernsdorfer, W. *Angew. Chem., Int. Ed.* **2005**, *44*, 2931.
(4) (a) Yachandra, V. K.; Sauer, K.; Klein, M. P. *Chem. Rev.* **1996**, *96*, 2927. (b) Yachandra, V. K.; Sauer, K. *Biochim. Biophys. Acta* **2004**, *1655*, 140.
(5) (a) Kok, B.; Forbrush, B.; McGloin, M. *Photochem. Photobiol.* **1970**, *11*, 457. (b) Haumann, M.; Liebisch, P.; Muller, C.; Barra, M.; Grabolle, M.; Dau, H. *Science* **2005**, *310*, 1019.
(6) (a) Debus, R. J. *Biochim. Biophys. Acta* **1992**, *1102*, 269. (b) Ruttinger, W.; Dismukes, G. C. *Chem. Rev.* **1997**, *97*, 1.
(7) Cinco, R. M.; Holman, K. L. M.; Robblee, J. H.; Yano, J.; Pizarro, S. A.; Bellacchio, E.; Sauer, K.; Yachandra, V. K. *Biochemistry* **2002**, *41*, 12928.
(8) (a) Ghanotakis, D. F.; Babcock, G. T.; Yocum, C. F. *FEBS Lett.* **1984**, *167*, 127. (b) Boussac, A.; Rutherford, A. W. *Biochemistry* **1988**, *27*, 3476.
(9) (a) Cinco, R. M.; Robblee, J. H.; Rompel, A.; Fernandez, C.; Yachandra, V. K.; Sauer, K.; Klein, M. P. *J. Phys. Chem. B* **1998**, *102*, 8248. (b) Cinco, R. M.; Robblee, J. H.; Messinger, J.; Fernandez, C.; Holman, K. L. M.; Sauer, K.; Yachandra, V. K. *Biochemistry* **2004**, *43*, 13271. (c) Kim, S. H.; Gregor, W.; Peloquin, J. M.; Brynda, M.; Britt, R. D. *J. Am. Chem. Soc.* **2004**, *126*, 7228. (d) Kargul, J.; Maghlaoui, K.; Murray, J. W.; Zsuzsanna, D.; Boussac, A.; Rutherford, A. W.; Vass, I.; Barber, J. *Biochim. Biophys. Acta* **2007**, *1767*, 404.
(10) (a) Ferreira, K. N.; Iverson, T. M.; Maghlaoui, K.; Barber, J.; Iwata, S. *Science* **2004**, *303*, 1831. (b) Iwata, S.; Barber, J. *Curr. Opin. Struct. Biol.* **2004**, *14*, 447.
(11) Loll, B.; Kern, J.; Saenger, W.; Zouni, A.; Biesiadka, J. *Nature* **2005**, *438*, 1040.
(12) Yano, J.; Kern, J.; Sauer, K.; Latimer, M. J.; Pushkar, Y.; Biesiadka, J.; Loll, B.; Saenger, W.; Messinger, J.; Zouni, A.; Yachandra, V. K. *Science* **2006**, *314*, 821.
(13) (a) Yano, J.; Kern, J.; Irrgang, K.; Latimer, M. J.; Bergmann, U.; Glatzel, P.; Pushkar, Y.; Biesiadka, J.; Loll, B.; Sauer, K.; Messinger, J.; Zouni, A.; Yachandra, V. K. *Proc. Natl. Acad. Sci. U.S.A.* **2005**, *102*, 12047. (b) Dau, H.; Liebisch, P.; Haumann, M. *Phys. Chem. Chem. Phys.* **2004**, *6*, 4781.
(14) (a) Mishra, A.; Wernsdorfer, W.; Abboud, K. A.; Christou, G. *Chem. Commun.* **2005**, 54. (b) Wang, W.; Zhang, X.; Chen, F.; Ma, C.; Chen, C.; Liu, Q.; Liao, D.; Li, L. *Polyhedron* **2005**, *24*, 1656. (c) Hewitt, I. J.; Tang, J.-K.; Madhu, N. T.; Clerac, R.; Buth, G.; Anson, C. E.; Powell, A. K. *Chem. Commun.* **2006**, 2650. (d) Jerzykiewicz, L. B.; Utko, J.; Duczmal, M.; Sobota, P. *Dalton Trans.* **2007**, 825.
(15) (a) Gil de Muro, I.; Insausti, M.; Lezama, L.; Pizarro, J. L.; Arriortua, M. I.; Rojo, T. *Eur. J. Inorg. Chem.* **1999**, 935. (b) Schauer, C. K.; Anderson, O. P. *Acta Crystallogr., Sect. C* **1988**, *44*, 981.
(16) Mishra, A.; Yano, J.; Pushkar, Y.; Yachandra, V. K.; Abboud, K. A.; Christou, G. *Chem. Commun.* **2007**, 1538.
(17) Wemple, M. W.; Tsai, H. L.; Wang, S.; Claude, J. P.; Streib, W. E.; Huffman, J. C.; Hendrickson, D. N.; Christou, G. *Inorg. Chem.* **1996**, *35*, 6437.

Table 1. Crystallographic Data for Complex **1**·12MeCN

color	dark red
formula	$C_{157}H_{141}Mn_{14}Sr_1N_{14}O_{50}$
MW (g mol^{-1})	3880.62
cryst syst	triclinic
space group	$P\bar{1}$
a (Å)	18.4417(16)
b (Å)	19.0430(16)
c (Å)	25.447(2)
α (deg)	69.789(2)
β (deg)	78.549(2)
γ (deg)	73.792(2)
Z	2
T (K)	173(2)
V (Å^3)	8001.2(12)
ρ_{calcd} (g cm^{-3})	1.611
radiation (Å)^a	0.71073
μ (cm^{-1})	8.825
all data	52550
unique data	35042
params^b	1750
final $R_1{}^{b,c}$	0.0896
final $wR_2{}^{b,c}$	0.2069

^{a} Mo Kα, graphite monochromator. ^{b} $I > 2\sigma(I)$. ^{c} $R_1 = \Sigma(\triangle F_o| - |F_c\triangle)/\Sigma|F_o|$. $wR_2 = [\Sigma[w(F_o{}^2 - F_c{}^2)^2]/\Sigma[w(F_o{}^2)^2]]^{1/2} S = [\Sigma[w(F_o{}^2 - F_c{}^2)^2]/(n - p)]^{1/2}$. $w = 1/[\sigma^2(F_o{}^2) + (mp)^2 + np]$, $p = [\max(F_o{}^2,0) + 2F_c{}^2]/3$, where m and n are constants.

graphite monochromator utilizing Mo Kα radiation ($\lambda = 0.71073$ Å). A suitable crystal of **1**·12MeCN was attached to a glass fiber using silicone grease and transferred to a goniostat, where it was cooled to 173 K for data collection. An initial search of reciprocal space revealed a triclinic cell; the choice of space group $P\bar{1}$ was confirmed by the subsequent solution and refinement of the structure. Cell parameters were refined using up to 8192 reflections. A full sphere of data (1850 frames) was collected using the ω-scan method (0.3° frame width). The first 50 frames were remeasured at the end of data collection to monitor instrument and crystal stability (maximum correction on I was <1%). Absorption corrections by integration were applied based on measured indexed crystal faces. The structures were solved by direct methods in SHELX-TL6,[18] and refined on F^2 using full-matrix least-squares. The non-H atoms were treated anisotropically, whereas H atoms were placed in calculated, ideal positions and refined as riding on their respective C atoms.

The asymmetric unit contains the complete SrMn$_{14}$ cluster and 12 MeCN molecules of crystallization. The latter were badly disordered and could not be modeled properly, thus program SQUEEZE,[19] a part of the PLATON[20] package of crystallographic software, was used to calculate the solvent disorder area and remove its contribution to the overall intensity data. A total of 1750 parameters were refined in the final cycle of refinement using 35042 reflections with $I > 2\sigma(I)$ to yield R_1 and wR_2 of 8.96 and 20.69%, respectively. Unit cell and structure refinement data are listed in Table 1.

EXAFS Studies. X-ray absorption spectroscopy (XAS) was performed at the Stanford Synchrotron Radiation Laboratory (SSRL) on beamline 9–3 at an electron energy of 3.0 GeV with an average current of 70–90 mA. The radiation was monochromatized by a Si(220) double-crystal monochromator. The intensity of the incident X-ray beam was monitored by a N$_2$-filled ion chamber (I$_0$) in front of the sample. XAS samples were made by carefully grinding 5–10 mg of compound and diluting it with a 10-fold excess of boron nitride. The mixture was packed into 0.5 mm thick sample holders and sealed with Mylar windows. The data were collected as fluorescence–excitation spectra with a Lytle detector.[21] Energy was calibrated by the pre-edge peak of KMnO$_4$ (6543.3 eV) for Mn XAS, and by the edge peak of strontium acetate (16120 eV) for Sr XAS. The standards were placed between two N$_2$-filled ionization chambers (I$_1$ and I$_2$) after the sample. The X-ray flux at 16–17 keV was between 2 and 5 × 10^9 photons s^{-1}mm^{-2} of the sample. The monochromator was detuned at 6600 eV to 50% of maximal flux to attenuate the X-ray second harmonic. Samples were kept at a temperature of 10 K in a liquid helium flow cryostat to minimize radiation damage. Data reduction is only briefly summarized here:[22] after conversion of background-corrected spectra from energy space to photoelectron wave vector (k) space, and weighted by k^3, a four-domain spline was subtracted for a final background removal (see the Supporting Information).

Other Studies. Infrared spectra were recorded in the solid state (KBr pellets) on a Nicolet Nexus 670 FTIR spectrometer in the 400–4000 cm^{-1} range. Elemental analyses (C, H and N) were performed by the in-house facilities of the University of Florida Chemistry Department. Variable-temperature dc and ac magnetic susceptibility data were collected at the University of Florida using a Quantum Design MPMS-XL SQUID susceptometer equipped with a 7 T magnet and operating in the 1.8–300 K range. Samples were embedded in solid eicosane to prevent torquing. Magnetization vs field and temperature data were fit using the program MAG-NET.[23] Pascal's constants were used to estimate the diamagnetic correction, which was subtracted from the experimental susceptibility to give the molar paramagnetic susceptibility (χ_M). Studies at ultralow temperatures (<1.8 K) were performed on single crystals at Grenoble using an array of micro-SQUIDs.[24] The high sensitivity of this magnetometer allows the study of single crystals on the order of 10 to 500 μm; the field can be applied in any direction by separately driving three orthogonal coils.

Results and Discussion

Synthesis. We recently began seeking synthetic routes to Ca/Mn, Sr/Mn and Ln/Mn (Ln = lanthanide) heterometallic complexes, and initial results from this effort have been very satisfying.[14a,3f] Our synthetic strategy has been to employ preformed manganese clusters such as [Mn$_3$O(O$_2$CR)$_6$(py)$_3$] (R = Me, Bu^t, Ph) and (NBu$^n_4$)[Mn$_4$O$_2$(O$_2$CPh)$_9$(H$_2$O)] and treat them with a heterometal carboxylate or other salt. A particularly attractive and easily prepared starting material is (NBu$^n_4$)[Mn$_4$O$_2$(O$_2$CPh)$_9$(H$_2$O)], which contains four Mn^{III} ions and only carboxylate and water ligands around the Mn/O core.[17] It therefore represents a good route to Mn^{III}- (and even Mn^{IV}-) containing products. We have thus been carrying out a thorough investigation of the reactions of the Mn$_4$ complex with various metal(II) salts, seeking new mixed-metal species. The following procedure with Sr was developed, which is similar to those used previously for Ca/Mn and Ln/Mn products.[14a,3f,k] Treatment of (NBu$^n_4$)[Mn$^{III}_4$-O$_2$(O$_2$CPh)$_9$(H$_2$O)] with 1 equiv of Sr(ClO$_4$)$_2$·xH$_2$O in

(18) Sheldrick, G. M. *SHELXTL6*; Bruker-AXS: Madison, WI, 2000.
(19) van der Sluis, P.; Spek, A. L. *Acta Crystallogr., Sect. A* **1990**, *46*, 194.
(20) Spek, A. L. *Acta Crystallogr., Sect. A* **1990**, *46*, C34.
(21) Cinco, R. M.; Robblee, J. H.; Rompel, A.; Fernandez, C.; Sauer, K.; Yachandra, V. K.; Mlein, M. P. *J. Synchrotron Radiat.* **1999**, *6*, 419.
(22) Robblee, J. H.; Messinger, J.; Cinco, R. M.; McFarlane, K. L.; Fernandez, C.; Pizarro, S. A.; Sauer, K.; Yachandra, V. K. *J. Am. Chem. Soc.* **2002**, *124*, 7459.
(23) Davidson, E. R. *MAGNET*; Indiana University: Bloomington, IN, 1999.
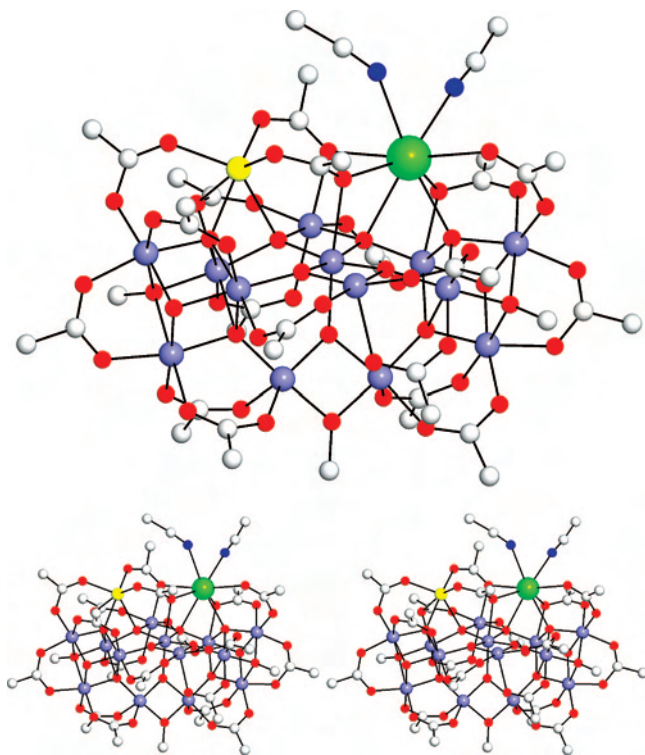(24) Wernsdorfer, W. *Adv. Chem. Phys.* **2001**, *118*, 99.

Figure 1. (Top) PovRay representation at the 50% probability level of the structure of **1**, and (bottom) a stereopair. Color scheme: Mn^{III}, light blue; Mn^{II}, yellow; Sr, green; O, red; N, dark blue; C, grey. For clarity, only ipso C atoms of phenyl rings are shown, and all H atoms have been omitted.

MeCN/MeOH (10:1 v/v) led to isolation of $[SrMn_{14}O_{11}$-$(OMe)_3(O_2CPh)_{18}(MeCN)_2]\cdot12MeCN$ (**1**$\cdot$12MeCN) in 55% yield (based on Mn). The Mn_4:Sr ratio of 1:1 was directed at a Mn_4Sr product as would be present in the WOC, and the small amount of MeOH was necessary to ensure solubility of $Sr(ClO_4)_2$. However, the absence of any chelating agents in the reaction solution allowed any smaller nuclearity intermediates to aggregate further and yield the $Mn_{14}Sr$ product **1**; reactions with added chelates such as 2,2′-bipyridine are under investigation. The reaction mixture is almost certainly a complicated mixture involving fragmentation, aggregation and redox processes, and the attainment of complex **1** in good yield and purity is undoubtedly facilitated by its crystallization directly from the reaction mixture. The presence of MeOH is common in much of our recent work,[25] and not only ensures solubility of all reactants but serves to (potentially) provide bridging ligands. Indeed, **1** is a new addition to the growing class of methoxide-bridged mixed-metal species,[14a,3f] although it should be added that **1** is the first mixed Sr/Mn molecular cluster of any type and with any ligation set.

Description of the Structure. A PovRay representation and a stereopair of **1** are presented in Figure 1, and its labeled core is shown in Figure 2. Selected interatomic distances are listed in Table 2.

Complex **1**$\cdot$12MeCN crystallizes in the triclinic space group $P\bar{1}$ with the $SrMn_{14}$ molecule in a general position. The structure consists of a $[SrMn_{14}O_{13}(OMe)_3]^{14+}$ core whose Mn ions are mixed valent ($13Mn^{III}$, Mn^{II}) and bridged by six μ_4-O^{2-}, five μ_3-O^{2-}, two μ_3-MeO^-, and one μ-MeO^- ions
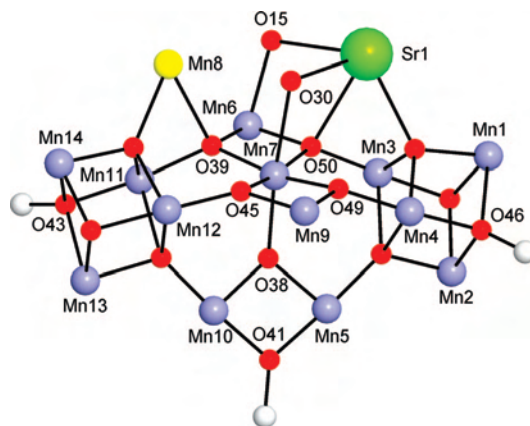

Figure 2. Labeled $[Mn_{14}SrO_{13}(OMe)_3]^{14+}$ core of complex **1**. Color scheme: Mn^{III}, light blue; Mn^{II}, yellow; Sr, green; O, red; C, grey. H atoms have been omitted for clarity.

Table 2. Selected Interatomic Distances (Å) for **1**

Mn3−O50	1.863(5)
Mn3−O48	1.905(5)
Mn3−O37	1.909(6)
Mn3−O21	1.935(6)
Mn3−O47	2.180(6)
Mn3−O6	2.265(7)
Mn6−O50	1.883(5)
Mn6−O39	1.902(5)
Mn6−O36	1.968(6)
Mn6−O22	1.974(5)
Mn6−O15	2.200(7)
Mn6−O33	2.236(7)
Mn7−O49	1.896(5)
Mn7−O45	1.908(5)
Mn7−O39	1.920(5)
Mn7−O50	1.933(5)
Mn7−O38	2.149(5)
Mn7−O30	2.486(10)
Mn8−O29	1.986(10)
Mn8−O16	2.150(8)
Mn8−O23	2.151(8)
Mn8-O44	2.271(6)
Mn8−O39	2.498(6)
Mn8−O35	2.505(6)
Mn9−O49	1.846(5)
Mn9−O45	1.861(5)
Mn9−O19	1.904(6)
Mn9−O12	1.953(6)
Mn9−O17	2.256(8)
Sr1−O30	2.501(6)
Sr1−O37	2.583(6)
Sr1−O6	2.607(7)
Sr1−O4	2.626(11)
Sr1−O15	2.685(7)
Sr1−N1	2.711(16)
Sr1−N2	2.763(17)
Sr1−O50	2.769(6)
Mn7···Mn9	2.8474(19)
Mn7···Sr1	3.7458(19)
Mn6···Mn7	2.8920(18)
Mn6···Sr1	3.839(2)
Mn3···Sr1	3.289(2)
Mn1···Mn3	2.825(2)
Mn1···Mn2	3.013(2)
Mn1···Mn4	3.0770(18)
Mn1···Sr1	3.9153(18)
Mn3···Mn4	3.0636(18)
Mn3···Sr1	3.289(2)

(Figure 2). The metal oxidation states and the protonation levels of O^{2-} and MeO^- ions were established by bond-valence sum calculations,[26] charge considerations, inspection
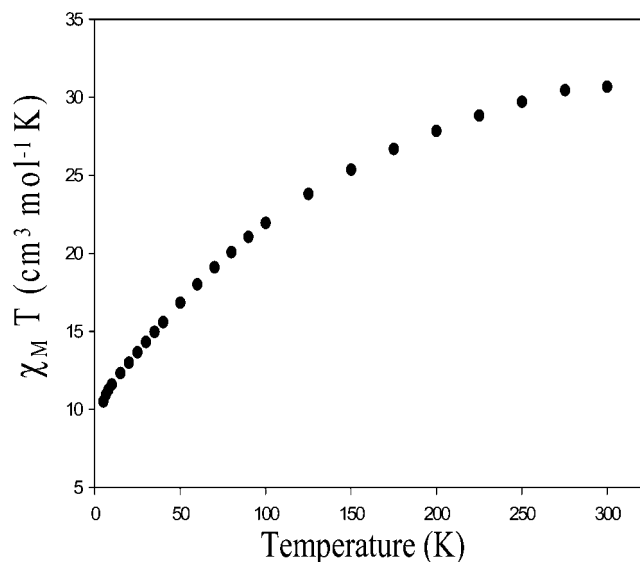
Figure 3. $\chi_M T$ *vs* T plot for complex **1**.

Figure 4. Magnetization (*M*) vs field (*H*) and temperature (*T*) data, plotted as reduced magnetization ($M/N\mu_B$) *vs* H/T, for complex **1** at applied fields of 0.1, 1.0, 2.0, 3.0, and 4.0 T and in the 1.8–10 K temperature range. The solid lines are the fit of the data; see the text for the fit parameters.

of metric parameters and the identification of Mn^{III} Jahn–Teller (JT) elongation axes. The core consists of two $[Mn_4O_3(OMe)]$ cubanes attached, via oxide bridges, on either side of a central, near linear, and planar $[Mn_3O_4]$ unit (Mn6, Mn7, Mn9). To the latter are also attached the Mn^{II} (Mn8) and Sr^{II} atoms above the central unit, and a $[Mn_2O(OMe)]$ rhombus (Mn5, Mn10) below it. Within this description, two triply bridging methoxides (O43, O46) lie within the two cubanes whereas the doubly bridging methoxide (O41) is within the $[Mn_2O(OMe)]$ rhombus. Peripheral ligation is provided by fourteen doubly and four triply bridging benzoates, as well as two terminal MeCN molecules on the Sr^{2+} ion. Three of the μ_3-$PhCO_2^-$ groups have one O atom doubly bridging a Sr^{II}/Mn^{III} pair, whereas the fourth benzoate has it bridging a Mn^{II}/Mn^{III} pair. Three of the Mn^{III} atoms (Mn5, Mn9, Mn10) are five-coordinate, whereas all the remaining Mn are six-coordinate. The Sr is eight-coordinate with six Sr-O bonds in the range 2.501–2.769 Å, and two Sr-N bonds to the two MeCN molecules of 2.711 and 2.763 Å. The closest Sr···Mn separation is 3.3 Å to Mn3.

DC Magnetic Susceptibility Studies. Solid-state, variable-temperature magnetic susceptibility measurements were performed on vacuum-dried, microcrystalline samples of complex **1**, restrained in eicosane to prevent torquing. The dc magnetic susceptibility (χ_M) data were collected in the 5.00–300 K range in a 1 kG (0.1 T) field, and they are plotted as $\chi_M T$ vs T in Figure 3. The $\chi_M T$ at 300 K is 30.67 cm^3 mol^{-1} K, much lower than the 43.38 spin-only value ($g = 2$) expected for a cluster comprising thirteen Mn^{III} and one Mn^{II} noninteracting ions, indicating extensive intramo-
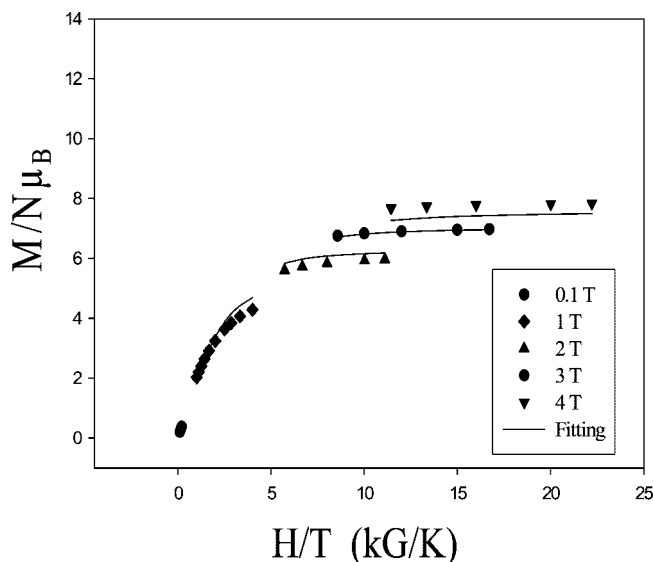
lecular antiferromagnetic interactions. The $\chi_M T$ steadily decreases further with decreasing temperature and finally reaches 10.51 cm^3 mol^{-1} K at 5.00 K, suggesting a small (but nonzero) ground-state spin, *S*. This was identified by collecting variable-temperature and -field magnetization (*M*) data in the 1.8–10 K and 0.1–4.0 T ranges. The data are plotted as reduced magnetization ($M/N\mu_B$) versus H/T in Figure 4 and fit, using the program MAGNET,[23] by matrix diagonalization assuming only the ground-state is populated, incorporating axial anisotropy ($D\hat{S}_z^2$) and Zeeman terms, and employing a full powder average. The corresponding Hamiltonian is given by eq 1

$$H = D\hat{S}_z^2 + g\mu_B\mu_0\hat{S}H \tag{1}$$

where *D* is the axial anisotropy constant, μ_B is the Bohr magneton, $\hat{S}_z$ is the easy-axis spin operator, *g* is the electronic *g* factor, and μ_0 is the vacuum permeability; the last term is the Zeeman energy associated with an applied magnetic field. The fit parameters were $S = 9/2$, $g = 1.88$, and $D = -0.50$ cm^{-1}. The *D* value of -0.5 cm^{-1} is consistent with the complex having predominantly Mn^{III} ions, and the $g < 2$ is as expected for Mn. When data collected at fields >4.0 T were included, a satisfactory fit could not be obtained. This is a common problem in high nuclearity Mn clusters, especially ones that contain Mn^{II} atoms, as a result of low-lying excited states; the fitting procedure assumes only a single state is occupied. Thus, we used for the fit only data collected at small fields, and a satisfactory fit was obtained (Figure 4) with the fit parameters given above.

To assess the precision of the fit parameters, the root-mean-square error surface for the fit was generated as a function of *g* and *D* using the program GRID.[27] The obtained error surface is depicted in the Supporting Information (Figure S1) as a 2-D contour plot, and the single minimum is observed at $g = 1.88$ and $D = -0.50$ cm^{-1}. The error surface

(25) (a) King, P.; Wernsdorfer, W.; Abboud, K. A.; Christou, G. *Inorg. Chem.* **2005**, *44*, 8659. (b) Stamatatos, T. C.; Foguet-Albiol, D.; Stoumpos, C. C.; Raptopoulou, C. P.; Terzis, A.; Wernsdorfer, W.; Perlepes, S. P.; Christou, G. *J. Am. Chem. Soc.* **2005**, *127*, 15380. (c) Tasiopoulos, A. J.; Wernsdorfer, W.; Abboud, K. A.; Christou, G. *Inorg. Chem.* **2005**, *44*, 6324.

(26) (a) Bond valence sum (BVS) calculations for the Mn ions of 1 gave values in the range 2.83–3.06 for the 13 Mn(III) ions. For the Mn(II) ion (Mn8) the value was 1.78. Also, for the three methoxides O41, O43, and O46 the values were 2.18, 1.88, and 1.93, respectively. (b) Liu, W.; Thorp, H. H. *Inorg. Chem.* **1993**, *32*, 4102.

(27) Davidson, E. R. *GRID*; Indiana University: Bloomington, IN, 1999.

near this minimum is rather soft (poorly defined) with an elongated contour line describing the region from $D = -0.45$ to -0.55 cm^{-1} and $g = 1.85$ to 1.91. This, together with the intrinsic uncertainties in determining D and g values from bulk magnetization data lead us to estimate the uncertainties in the fit parameters as $D = -0.50(5)$ cm^{-1} and $g = 1.88(10)$.

Although **1** has a relatively small ground state of $S = 9/2$, the large D value of -0.5 cm^{-1}, which is comparable to Mn$_4$[28] and Mn$_{12}$ SMMs,[2] suggested that the barrier to magnetization relaxation might be large enough for **1** to function as an SMM. The S and D values suggest an upper limit to the barrier (U) to magnetization reversal of $U = (S^2 - \frac{1}{4})|D| = 10$ cm$^{-1} = 14$ K,[1] although the actual, effective barrier (U_{eff}) will be smaller due to quantum tunneling of the magnetization (QTM). Thus, AC susceptibility measurements were performed to investigate whether **1** might be an SMM or not.

AC Magnetic Susceptibility Studies. AC studies were performed in the 1.8–10 K range in a zero DC field and a 3.5 G AC field oscillating at frequencies in the 10–1000 Hz range. A decrease in the ac in-phase (χ_M') susceptibility signal and a concomitant increase in the out-of-phase (χ_M'') signal are indicative of the onset of the slow, superparamagnet-like relaxation of SMMs.[1,2] The data for complex **1** (Figure 5) exhibit below 3 K the frequency-dependent tails of χ_M'' signals whose peak maxima clearly lie at temperatures below the operating minimum of our SQUID magnetometer (1.8 K). These χ_M'' signals are accompanied by a concomitant frequency-dependent decrease in the in-phase signals (shown as $\chi_M'T$).

In the absence of slow relaxation, the ac in-phase $\chi_M'T$ signal should be equal to the dc $\chi_M T$, and this provides an additional, independent means of obtaining the ground state S value without the potential complications of an applied dc field. Figure 5 shows that $\chi_M'T$ is decreasing at temperatures <10 K, consistent with the depopulation of excited states with S greater than that of the ground state. Below ~6 K, the line begins to slope more steeply and then drops rapidly below 3 K as a result of slow relaxation effects, consistent with the concomitant appearance of frequency-dependent out-of-phase χ_M'' signals (Figure 5, bottom). Some of the decrease in $\chi_M'T$ in the 3–6 K region is likely due to weak intermolecular interactions. Thus, we extrapolated the plot from above 6 K down to 0 K, where only the ground-state would be populated, and this gave $\chi_M'T \approx 10.5$ cm^3 mol^{-1} K. This is in satisfying agreement with the $S = 9/2$ and $g = 1.88$ value obtained from the dc magnetization fit, which predicts $\chi_M'T = 10.9$ cm^{3}Kmol^{-1}. Note that an $S = 7/2$ or 11/2 ground-state would give a $\chi_M'T$ of 6.96 or 15.8 cm^3 mol^{-1} K, respectively, for $g = 1.88$ (or $\chi_M'T = 7.9$ or 17.9 cm^3 mol^{-1} K, respectively, for $g = 2.0$), both in disagreement with the experimental data in Figure 5. The AC data thus
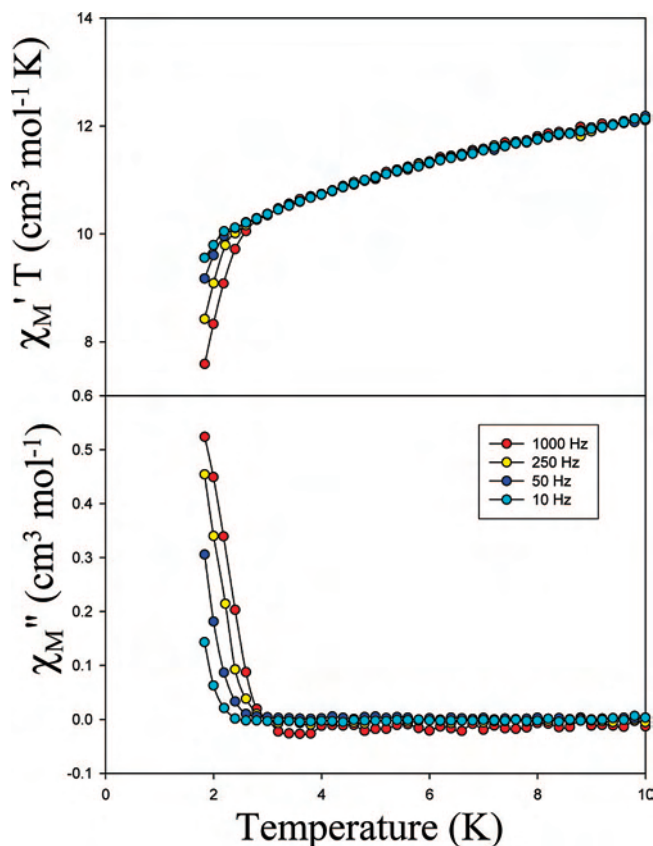

Figure 5. AC susceptibility of complex **1** in a 3.5 G field oscillating at the indicated frequencies: (top) in-phase signal (χ_M') plotted as $\chi_M'T$ vs T; and (bottom) out-of-phase signal χ_M'' vs T.

provide an independent confirmation of an $S = 9/2$ ground state for complex **1**.

Hysteresis Studies below 1.8 K. The frequency-dependence in the $\chi_M'T$ and χ_M'' signals below 3 K in Figure 5 suggested that complex **1** might be a SMM. To explore this further, we collected magnetization versus applied DC field data down to 0.04 K on single crystals of **1**·12MeCN, which had been kept in contact with their mother liquor, using a micro-SQUID instrument, with the field approximately along the easy axis (z axis) of the molecule.[24] Magnetization vs field hysteresis, the diagnostic property of a magnet, was indeed observed below 1.3 K (Figure 6). The hysteresis loops exhibit increasing coercivity with increasing field sweep rate at a constant temperature (Figure 6, bottom), and increasing coercivity with decreasing temperature at a constant sweep rate (Figure 6, top), as expected for the superparamagnet-like properties of a SMM. These loops thus confirm complex **1** to be a new addition to the family of SMMs. The blocking temperature (T_B) is ~1.4 K, above which there is no hysteresis.

The most dominating feature of the hysteresis loops in Figure 6 is the large step at zero field due to quantum tunneling of the magnetization (QTM) through the anisotropy barrier, with a second step at ~1 T. The large zero-field step indicates that QTM in zero field is fast, and this in turn is consistent with the low symmetry of the molecule, which introduces a nonzero rhombic (transverse) anisotropy into the spin Hamiltonian i.e. $E(\hat{S}_x^2 - \hat{S}_y^2)$, where E is the rhombic

(28) (a) Wang, S.; Folting, K.; Streib, W. E.; Schmitt, E. A.; McCusker, J. K.; Hendrickson, D. N.; Christou, G. *Angew. Chem., Int. Ed.* **1991**, *30*, 305. (b) Andres, H.; Basler, R.; Gudel, H.-U.; Aromi, G.; Christou, G.; Buttner, H.; Ruffle, B. *J. Am. Chem. Soc.* **2000**, *122*, 12469. (c) Wemple, M. W.; Tsai, H.-L.; Folting, K.; Hendrickson, D. N.; Christou, G. *Inorg. Chem.* **1993**, *32*, 2025. (d) Wang, S.; Tsai, H.-L.; Folting, K.; Streib, W. E.; Hendrickson, D. N.; Christou, G. *Inorg. Chem.* **1996**, *35*, 7578.
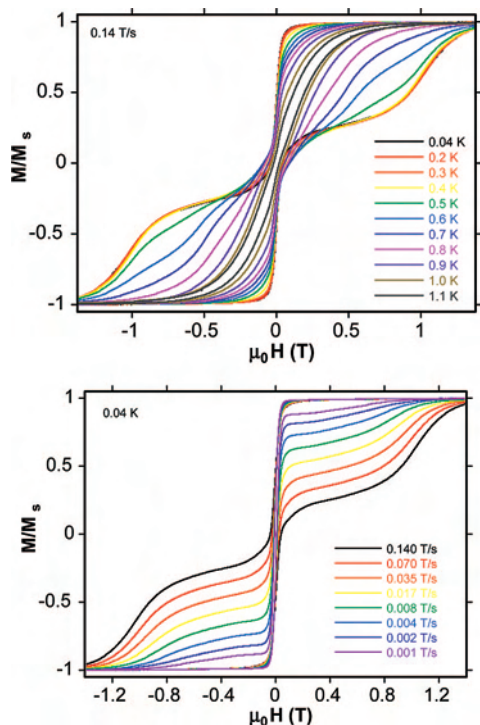
Figure 6. Magnetization (*M*) vs DC field (*H*) hysteresis loops for a single crystal of **1**·12 MeCN: (top) at the indicated temperatures and a fixed field sweep rate of 0.14 T/s; and (bottom) at the indicated field sweep rates and a fixed temperature of 0.04 K. The magnetization is normalized to its saturation value, M_S.
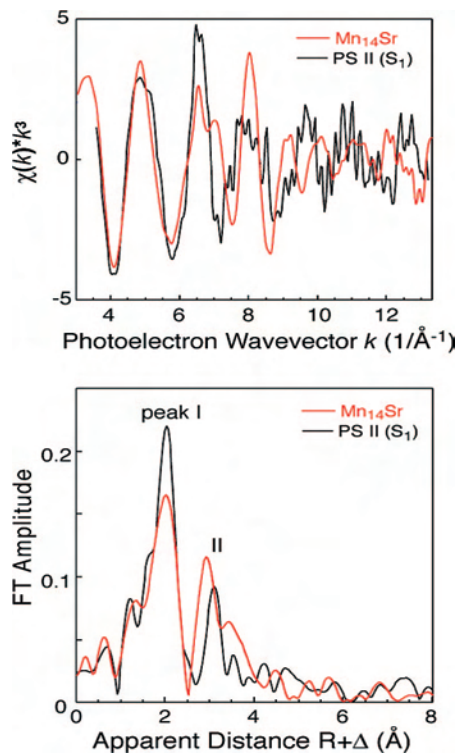

Figure 7. (Top) k^3-weighted Sr K-edge EXAFS spectra of Mn$_{14}$Sr complex **1** (red) and Sr- reactivated PS II samples in the S$_1$ state (black).[9a] (Bottom) Fourier transforms of the averaged Sr K-edge EXAFS spectra for complex **1** (red) and Sr-reactivated PS II samples in the S$_1$ state (black).[9a]

zero-field splitting parameter. The greater is the transverse anisotropy, the greater will be the mixing of levels on either side of the anisotropy barrier, leading to increased rates of

QTM. The fast relaxation at zero field precludes magnetization decay vs time studies to provide relaxation rate vs *T* kinetic data; we cannot therefore construct an Arrhenius plot from which could be determined the effective barrier to magnetization relaxation, U_{eff}.

Sr EXAFS Spectroscopy. Complex **1** is the first molecular Sr/Mn complex and the opportunity was therefore taken to characterize the EXAFS signature of a Sr atom in a structurally characterized mixed-metal, oxide-bridged Sr/Mn complex. This also makes such data available for comparison with analogous data on the Sr-substituted WOC, a Sr/Mn/O species. As stated earlier, Sr EXAFS studies on the latter indicate a Sr···Mn separation of ∼3.5 Å, very slightly longer than the ∼3.4 Å Ca···Mn separation in the native WOC.[9,7]

The Sr K-edge EXAFS (k^3-weighted) spectra of **1** and Sr-substituted WOC in the resting (S$_1$) state[9a] are shown in Figure 7 (top), and the Fourier transforms in Figure 7 (bottom). Each peak in the FT spectrum indicates a radial distribution of atoms surrounding the Sr atoms in **1** and appears at distances shorter than the actual Sr-backscatterer distances due to an average phase shift induced by the potentials of the given absorber-scatterer pair on the photo-electron. The first Fourier peak is from the first shell of ligands about Sr (O and/or N backscatters), and the second Fourier peak is from Sr···Mn separations. Although there are three of the latter (3.3, 3.7, and 3.9 Å) in **1**, only the shorter vectors (3.3 and 3.7 Å) are the dominant feature in the FT peak. The second peak of the PS II spectrum (black) in Figure 7 (bottom) is clearly shifted to a longer distance compared to **1**, which agrees with the fact that the Sr···Mn distance in Sr-substituted PS II was earlier reported to be 3.5 Å,[9a] longer than the shortest Sr···Mn vector in **1** (3.3 Å). The higher intensity of the second peak in Sr-substituted PS II compared to the shoulder for complex **1** is likely due to the presence of more than one Sr···Mn interaction in the former, as suggested by recent crystallographic data on PS II,[11,12] where three Ca···Mn separations were postulated. The Fourier peaks I and II were isolated separately and simulated with Sr−ligand (2.5–2.7 Å) and Sr···Mn (>3.3 Å) distances (see the Supporting Information, Table S1). Fit I-1 of Table S1 attempts to fit peak I with only Sr−O interactions, while Fit I-2 includes both Sr−O and Sr−N interactions. A noticeable improvement in fit quality was observed when peak I was fit using the coordination number (*N*) from the crystal structure data. The coordination number of Sr deviates from the true *N* (six Sr−O and two Sr−N bonds) by less than 10% when unconstrained. Peak II, which clearly contains at least two components, was fit to multiple Sr···Mn distances; as stated above, there are three Sr···Mn interactions (3.3, 3.7, and 3.9 Å) in the crystal structure. If complex **1** was treated as an unknown structure with two-shell Sr···Mn interactions (Fit II-1), the total *N* value (*N* = 1.4 for 3.34 Å, and *N* = 1.2 for 3.72 Å) is between 2 to 3, indicating at least two Sr···Mn interactions. Increasing the number of shells from two to three (Fit II-2) with fixed N values obtained from the crystal structure data significantly improved the fit quality. In comparison to **1**, the second peak of the Sr-substituted PS II S$_1$ state shows a single FT peak
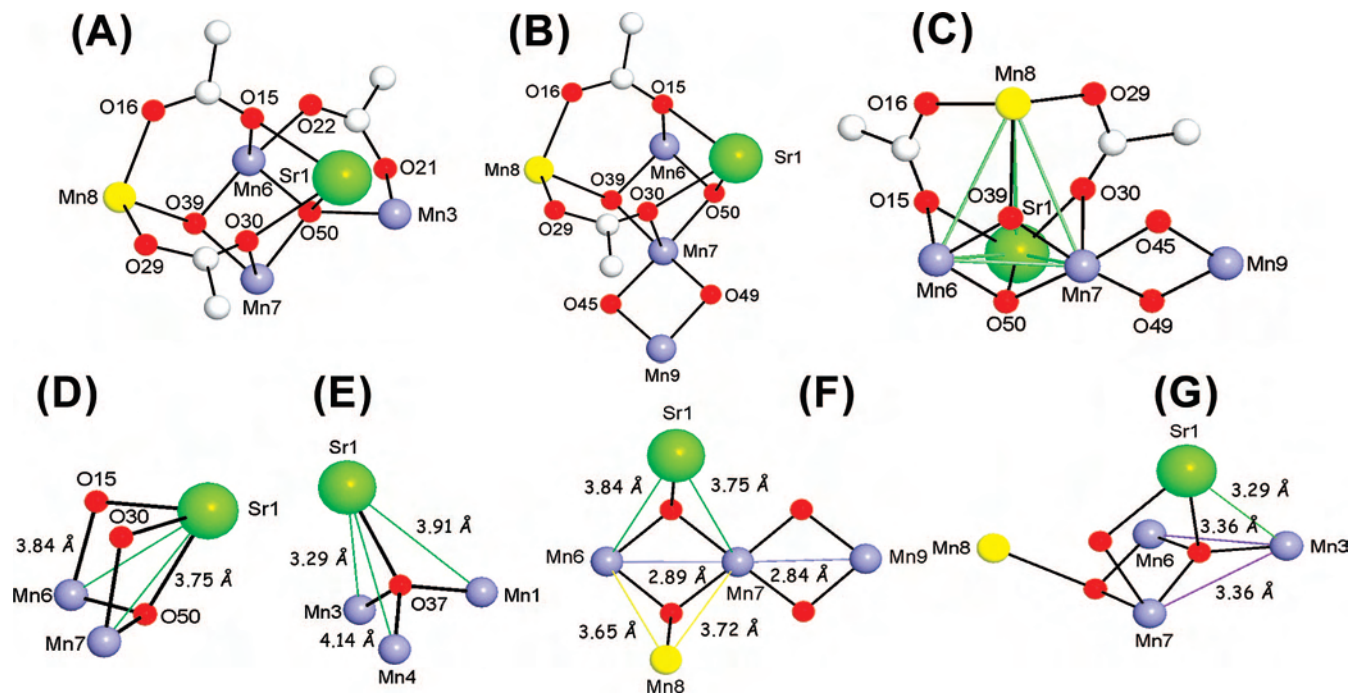
Figure 8. PovRay representations at the 50% probability level of subfragments within **1**. (A) and (B) depict two "open-cubane" subunits: (A) extrinsic Mn (Mn3) attached to an oxide of the open-cubane; (B) extrinsic Mn (Mn9) attached to two extrinsic μ-O^{2-} ions. (C) Subunit that resembles that in the 3.0 Å crystal structure of the WOC.[11] (F, G) Metal−metal separations within the (A, B, C) subunits. (D, E) Subunits that resemble the structure of the WOC obtained from polarized EXAFS data.[12] Color scheme: Mn^{III}, light blue; Mn^{II}, yellow; Sr, green; O, red; C, grey.

at 3.5 Å.[9a] This was best fit to two Sr···Mn interactions (N = 2) with similar fitting parameters (σ^2 and S_0^2).

The structure of **1** contains several subfragments of potential relevance to the species in the Sr-substituted WOC. Figure 8 (A and B) show two such $SrMn_4$ subunits with an open-cubane topology. All Sr···Mn and close Mn···Mn separations are listed in Table 2, and some are also shown in Figure 8 (F and G). Although the study by Ferreira et al. at 3.5 Å suggests[10] that the WOC might have a $CaMn_3O_4$ cubane linked to a fourth Mn atom, the earlier X-ray studies at 3.8 and 3.7 Å resolution postulated[29] that the four Mn ions are arranged in a "3 + 1" (i.e., open-cubane) fashion. Thus, the subunits of **1** in Figure 8 (A and B) have some intriguing similarity to the structural models proposed from the crystallographic studies of the WOC S_1 state. Another view of one of these subunits (Figure 8B) is shown in Figure 8C, highlighting the $SrMn_3$ pyramid (green lines) connected to the extrinsic Mn9. This arrangement of metal atoms is comparable to the most recent crystallographic study of the S_1 state of the WOC of PS II at 3.0 Å in which the aforementioned model was proposed.[11]

Last year, a new set of models for the WOC was proposed based on polarized EXAFS and X-ray diffraction data.[12] Figure 8 (D and E) show subunits within **1** that correspond to ones in this proposed structure of the WOC.[12] Figure 8D contains two rhombs (Sr1, O30, Mn7, O50, and Sr1, O15, Mn6, O50), which are fused along the Sr1−O50 bond. These rhombs contain monoatomic di-μ-oxide-bridges (O30, O15) between the Sr and Mn. More intriguingly, Figure 8E depicts

a distorted tetrahedral subunit containing a single-atom oxide bridge (O37) between the Sr and Mn ions, exactly as proposed in the most recent WOC model,[12] wherein the Ca atom is similarly linked to three Mn atoms. It is thus perhaps not surprising that the FT peak positions and the intensity observed in the Sr EXAFS spectrum for **1** in Figure 7 bear some similarity to those of the S_1 state of PS II, because it is possible that the local ligand and structural environment that the Sr atom of complex **1** finds itself in might well be very similar to that of the Sr atom in the biological site, even though, of course, the overall nuclearity of the $SrMn_{14}$ complex is much higher than that of the native site.

We also carried out Mn EXAFS studies on complex **1**, and these data, pertinent figures, and discussion are available in the Supporting Information.

Summary and Conclusions

The first molecular Sr/Mn complex has been synthesized via a straightforward procedure starting employing easily obtained starting materials. Complex **1** is of metal nuclearity $SrMn_{14}$ and has an $S = 9/2$ ground state, as well as significant magnetoanisotropy as reflected in an axial ZFS parameter, D, of magnitude -0.5 cm^{-1}. These two facts together lead to **1** possessing a sufficient barrier to magnetization relaxation to exhibit slow relaxation rates at low temperatures and thus to be a new member of the growing family of single-molecule magnets (SMMs). This was confirmed by observation of hysteresis loops in magnetization vs applied dc field scans. The fact that **1** is the first molecular Sr/Mn complex is also of some interest from a bioinorganic viewpoint. Because it contains a single Sr atom, Sr EXAFS studies have been carried out, and these have allowed some comparisons with those on Sr-

(29) (a) Zouni, A.; Witt, H. T.; Kern, J.; Fromme, P.; Krauss, N.; Saenger, W.; Orth, P. *Nature* **2001**, *409*, 739. (b) Kamiya, N.; Shen, J. R. *Proc. Natl. Acad. Sci. U.S.A.* **2003**, *100*, 98.

substituted WOC samples. The overall conclusion is that the local Sr environment in the model complex **1** has some similarities, but also differences, with that of the biological site. In any event, it is useful to finally have some Sr EXAFS data available on a structurally characterized oxide-bridged Sr/Mn complex to act as a benchmark for this technique.

Supporting Information Available: X-ray crystallographic files in CIF format for complex **1**·12MeCN; magnetization fit error surface and details of EXAFS analysis and fitting (PDF). This material is available free of charge via the Internet at http://pubs.acs.org.

IC701339P